iScience

CellPress
OPEN ACCESS

Article

The selective norepinephrine reuptake inhibitor reboxetine promotes late-stage fracture healing in mice

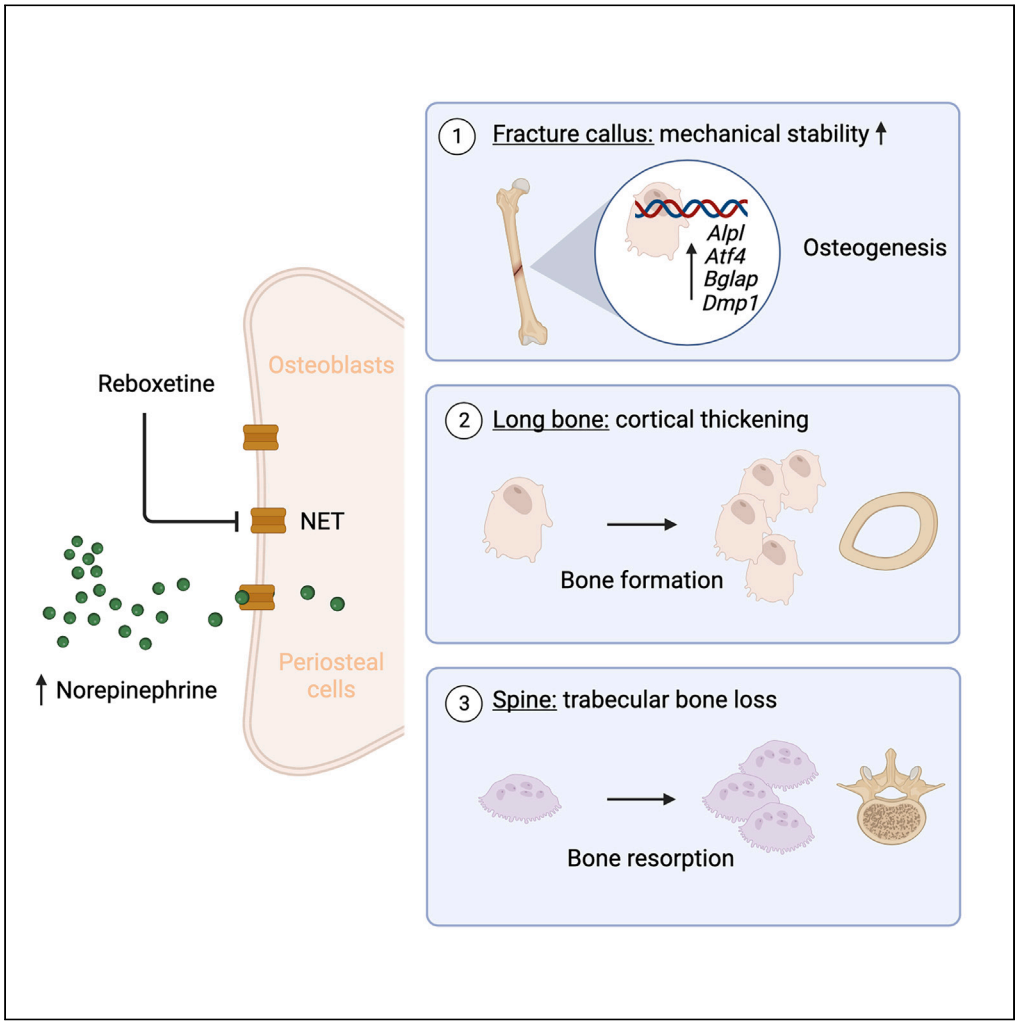

Antonia Donat, Shan Jiang, Weixin Xie, ..., Serafeim Tsitsilonis, Anke Baranowsky, Johannes Keller

j.keller@uke.de

Highlights

The SNRI reboxetine decreases bone volume in the spine in mice with femoral fractures

Reboxetine increases femur cortical thickness in mice with contralateral fractures

Reboxetine improves late-stage fracture healing through promoting osteogenesis

Donat et al., iScience 26, 107761
October 20, 2023
https://doi.org/10.1016/j.isci.2023.107761

iScience

CellPress
OPEN ACCESS

Article

The selective norepinephrine reuptake inhibitor reboxetine promotes late-stage fracture healing in mice

Antonia Donat,[1] Shan Jiang,[1] Weixin Xie,[1] Paul Richard Knapstein,[1] Lilly-Charlotte Albertsen,[1] Judith Luisa Kokot,[1] Jan Sevecke,[1] Ruben Augustin,[1] Denise Jahn,[2,3] Timur Alexander Yorgan,[4] Karl-Heinz Frosch,[1,5] Serafeim Tsitsilonis,[2,3] Anke Baranowsky,[1] and Johannes Keller[1,6,*]

SUMMARY

Impaired fracture healing is of high clinical relevance, as up to 15% of patients with long-bone fractures display non-unions. Fracture patients also include individuals treated with selective norepinephrine reuptake inhibitors (SNRI). As SNRI were previously shown to negatively affect bone homeostasis, it remained unclear whether patients with SNRI are at risk of impaired bone healing. Here, we show that daily treatment with the SNRI reboxetine reduces trabecular bone mass in the spine but increases cortical thickness and osteoblast numbers in the femoral midshaft. Most importantly, reboxetine does not impair bone regeneration in a standardized murine fracture model, and even improves callus bridging and biomechanical stability at late healing stages. In sum, reboxetine affects bone remodeling in a site-specific manner. Treatment does not interfere with the early and intermediate stages of bone regeneration and improves healing outcomes of the late-stage fracture callus in mice.

INTRODUCTION

The skeleton is constantly being remodeled by the activity of bone-resorbing osteoclasts and bone-forming osteoblasts. In the healthy, weight bearing skeleton, only gross forces may inflict injury to the bone with a resulting fracture. After a fracture occurs, bone regeneration, an evolutionary highly preserved process, allows the scarless healing of the injured bone. Similar to bone remodeling, the balanced activity of osteoclasts and osteoblasts is essential for adequate remodeling of the fracture callus and overall outcome of bone healing. However, despite treatment according to best practice nowadays, risks still range between 10 and 15% that the bone will not heal, resulting in fracture non-union.[1,2] Impaired bone healing exerts a severe burden on affected patients, as they require multiple revision surgeries, are prone to further complications (e.g., infection), and experience prolonged immobilization and inability to work.[3,4]

Both bone remodeling and regeneration are regulated by common key factors, including mechanical load, hormones, and cytokines amongst many others. Research in the past two decades has provided ample evidence that bone remodeling is also controlled by nerves and locally released neurotransmitters. In particular, the sympathetic nervous system was shown to potently affect both osteoclast and osteoblast function.[5,6] The current model of how peripheral sympathetic nerves affect the skeleton includes the release of norepinephrine (NE), which then binds to the beta 2 adrenoreceptor expressed on osteoblasts. This leads to an inhibition of osteoblast proliferation and an induction of pro-resorptive RANKL, overall resulting in decreased bone formation and increased bone resorption.[7] Apart from alterations in sympathetic tone, NE levels in bone are also regulated by the NE transporter (NET), which, in addition to presynaptic neurons, is also expressed in bone cells.[8] In this regard it was demonstrated that osteoblasts and osteocytes exhibit NE uptake activity via NET and can catabolize but not generate NE.[9]

From a pharmacological perspective, NET is a principal target of drugs used for the treatment of psychiatric disorders such as depression, anxiety or attention deficit hyperactivity disorders.[10–12] Based on NET expression in osseous tissue, clinical concerns have been raised about potential adverse effects of NET inhibitors regarding skeletal health. In fact, mice with genetic inactivation of NET, or pharmacologic blockade of NET via the selective norepinephrine reuptake inhibitor (SNRI) reboxetine, were reported to display trabecular bone loss due to decreased

[1]Department of Trauma and Orthopedic Surgery, University Medical Center Hamburg-Eppendorf, 20251 Hamburg, Germany
[2]Center for Musculoskeletal Surgery, Charité-Universitätsmedizin Berlin, Corporate Member of Freie Universität Berlin and Humboldt-Universität zu Berlin, 13353 Berlin, Germany
[3]Berlin Institute of Health at Charité-Universitätsmedizin Berlin, Julius Wolff Institute, 13353 Berlin, Germany
[4]Department of Osteology and Biomechanics, University Medical Center Hamburg-Eppendorf, 20251 Hamburg, Germany
[5]Department of Trauma Surgery, Orthopedics and Sports Traumatology, BG Hospital Hamburg, 21033 Hamburg, Germany
[6]Lead contact
*Correspondence: j.keller@uke.de
https://doi.org/10.1016/j.isci.2023.107761

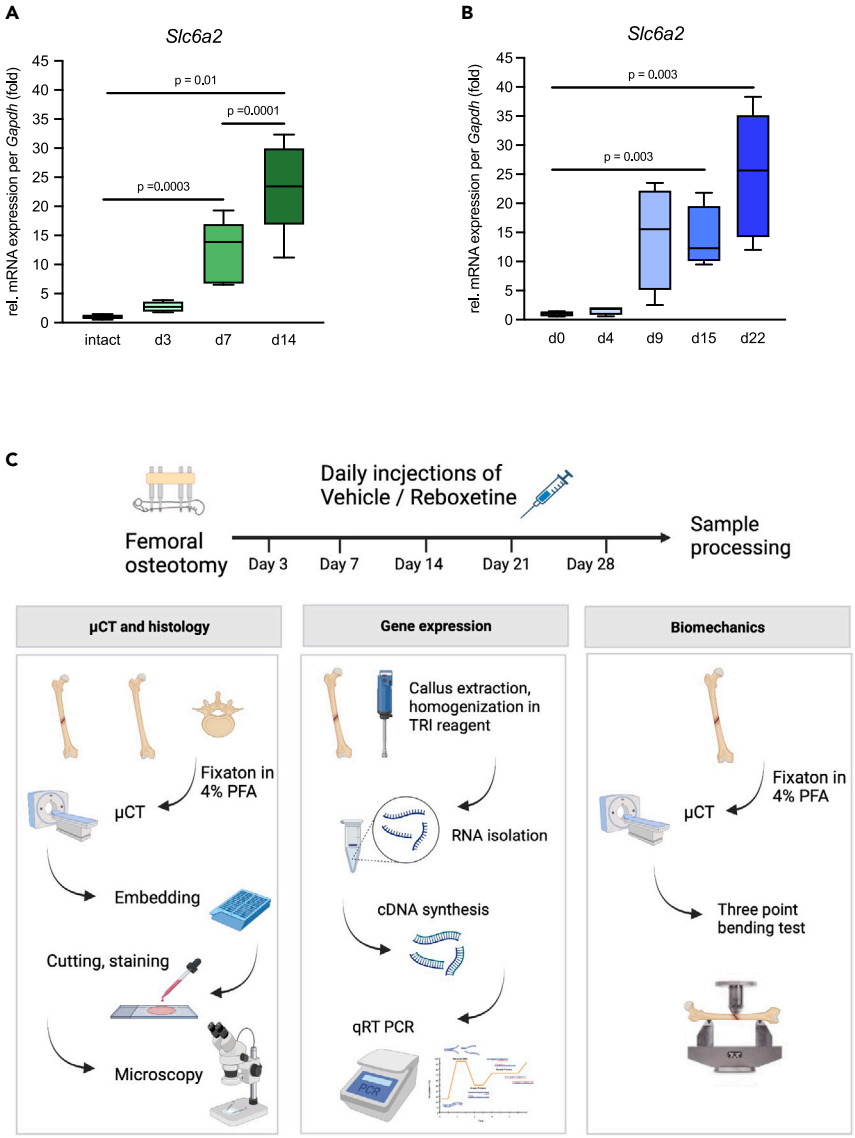

Figure 1. Expression of the norepinephrine transporter Slc6a2 increases during bone healing

(A and B) (A) qRT-PCR of NET expression (encoded by *Slc6a2*) in the fracture callus (n = 6 mice) compared to intact femoral bone (n = 6 sham operated mice; corresponding midshaft area), and (B) in periosteal cells (n = 6 independent cultures) undergoing osteogenic differentiation at the indicated time. Non-parametric Mann–Whitney U test, data are shown in boxplots with median, 25th and 75th quantiles. Whiskers indicate upper and lower extremes, respectively. (C) Schematic representation of the study protocol and respective algorithm for sample assessment.

bone formation and an enhanced bone resorption.[9] Although solid evidence is still lacking due to only a limited number of studies, available clinical data suggests that patients prescribed SNRI display an increased fracture risk.[13]

Although accumulating evidence supports a pivotal role of NET in the regulation of bone remodeling, its impact on bone regeneration is unknown. However, this is especially relevant in orthopedic trauma surgery, as a considerate proportion of fracture patients are prescribed with SNRI.[14] In the current study, we thus hypothesized that SNRI application impairs fracture healing and results in an increased rate of fracture non-union in mice.

RESULTS

Expression of the norepinephrine transporter Slc6a2 increases during bone healing

To investigate a possible role of reboxetine in bone regeneration, we first monitored expression of NET, encoded by *Slc6a2* and representing the principal target of reboxetine, during bone healing. While expressed at comparatively low levels in the midshaft of non-fractured femora, *Slc6a2* expression dramatically increased in the callus throughout the course of bone healing (Figure 1A). Likewise, *ex vivo* generated

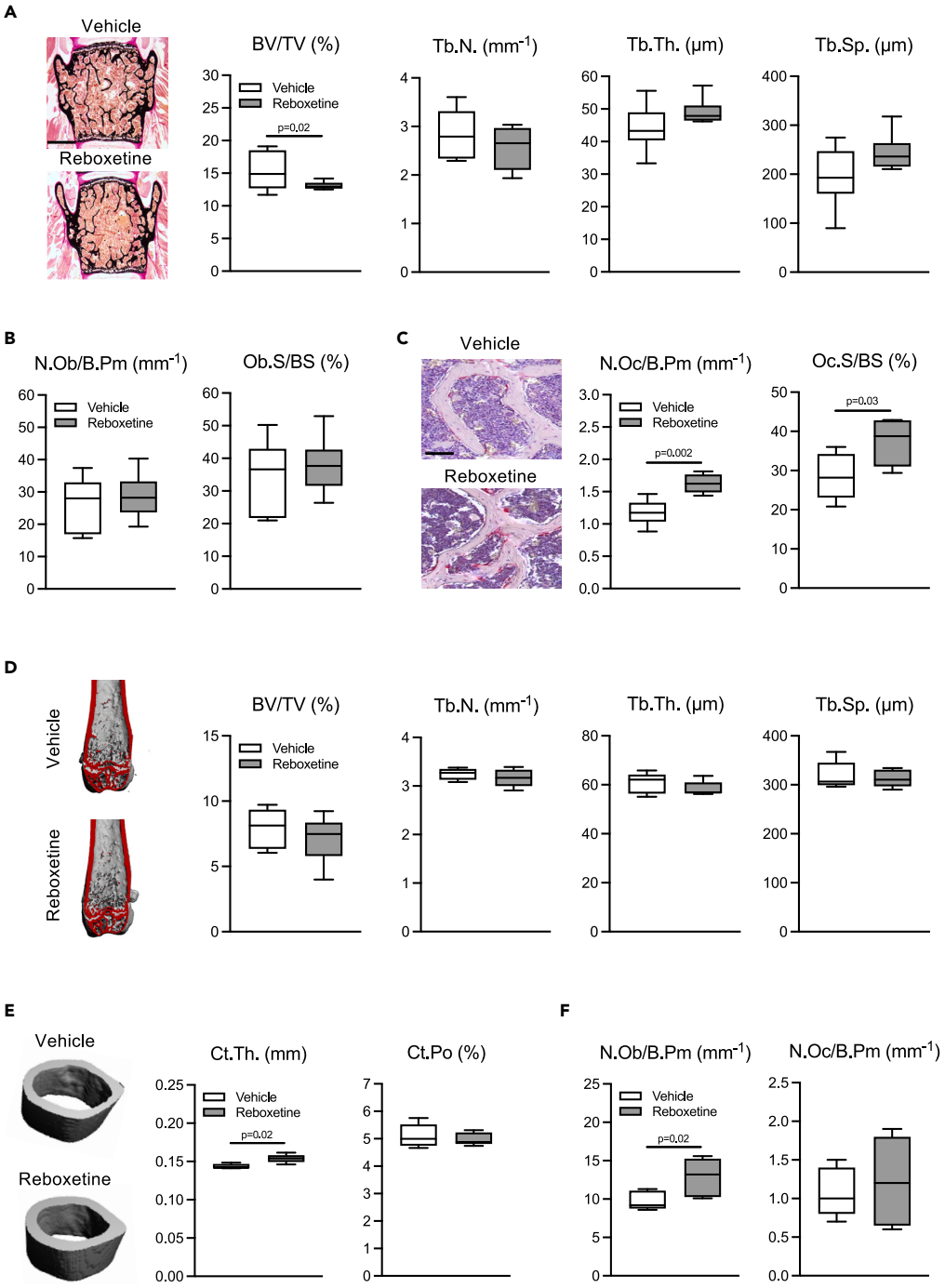

Figure 2. Systemic reboxetine treatment exerts distinct effects in the non-fractured skeleton

(A) Left: Representative von Kossa/van Gieson staining of undecalcified vertebra sections (L4) following 21 days of treatment with reboxetine (15 mg kg^{-1}) or vehicle in mice with a femoral fracture. Scale bar = 500 µm. Right: Histomorphometric quantification of the indicated structural bone parameters in the same groups. BV/TV = bone volume per tissue volume, Tb.N. = trabecular number, Tb.Th. = trabecular thickness, Tb.Sp. = trabecular separation.

(B) Histomorphometric quantification of the indicated cellular parameters of bone formation. N.Ob/B.Pm = osteoblast numbers per bone perimeter, Ob.S/BS = osteoblast surface per bone surface.

(C) Histomorphometric quantification of the indicated cellular parameters of bone resorption. N.Oc/B.Pm = osteoclast numbers per bone perimeter, Oc.S/BS = osteoclast surface per bone surface. Representative TRAP-stained vertebra sections are displayed in the left. Scale bar = 50 µm.

(D) Representative µCT images of the non-fractured, distal femur and quantification of trabecular bone volume per tissue volume in addition to trabecular number, thickness and separation after 21 days of treatment with reboxetine (15 mg kg^{-1}) or vehicle in mice with a contralateral femoral fracture.

Figure 2. *Continued*

(E) Representative μCT images of the midshaft non-fractured femur, and quantification of cortical bone parameters in the same groups. Ct.th. = cortical thickness, Ct.Po = cortical porosity.

(F) Osteoblast and osteoclast numbers in the midshaft non-fractured femur of the same mice. n = 6 mice per group. Unpaired Student's *t* test, data are shown in boxplots with median, 25th and 75th quantiles. Whiskers indicate upper and lower extremes, respectively.

periosteal cells undergoing osteogenic differentiation displayed a steadily increasing expression of *Slc6a2* (Figure 1B). As these observations suggested a possible role of NE reuptake in fracture healing, we subjected mice to a femoral osteotomy stabilized by an external fixator. At the day of surgery, daily systemic injections with reboxetine or vehicle were initiated and continued until sacrifice, when fractured and non-fractured bone samples were collected at pre-determined time points representing the early, intermediate, and late stages of bone healing (Figure 1C). In line with previous reports in mice lacking Slc6a2 globally,[9] increased serum levels of NE were detected in mice treated with reboxetine for 3 weeks (Figure S1A). In addition, increased expression of *uncoupling protein 1* (*Ucp1*) was detected in the fracture callus 3 days following osteotomy in treated mice, indicative of enhanced NE signaling (Figure S1B).

Systemic reboxetine treatment exerts distinct effects in the non-fractured skeleton

Previously it was shown that systemic reboxetine treatment decreases trabecular bone mass. Therefore, to assess the pharmaceutical efficacy of our chosen approach, we first analyzed bone architecture in the intact skeleton, including the spine and the contralateral non-fractured femur. While trabecular number, thickness and separation where not significantly altered, we observed a decrease in bone volume per tissue volume in undecalcified spine sections derived from mice treated with reboxetine 21 days following surgery (Figure 2A). Similar observations were made using μCT scanning of spine samples, which revealed a decrease in bone volume per tissue volume and trabecular number in the reboxetine group (Figure S2A). Histomorphometrically, osteoblast parameters, indicative of bone formation, were unaffected, however, a significant increase in both osteoclast numbers and surface was detected as a potential explanation (Figures 2B and 2C). In the distal femur, reboxetine treatment was not associated with alterations in trabecular bone architecture or an alteration in cellular osteoblast and osteoclast parameters (Figures 2D and S2B). In contrast, while osteocyte numbers were unaltered (Figure S2C), an increased cortical thickness, accompanied by normal cortical porosity, was detected in the femoral midshaft of reboxetine-treated mice (Figure 2E). Here, histomorphometric assessment revealed an elevation in endocortical osteoblast numbers, whereas osteoclast numbers were unaffected (Figure 2F). These results confirmed the pharmacological efficacy of reboxetine administration and demonstrated a site-specific skeletal impact of reboxetine.

Reboxetine does not impair the early and intermediate stages of fracture healing and is associated with increased cellular indices of bone formation in the fracture callus

Using μCT scanning, we next monitored osseous callus formation at early (day 7 and 14) and intermediate (day 21) time points after surgery. A regular course of callus mineralization was observed in mice treated with reboxetine (Figure 3A). Quantification of radiologic callus parameter revealed neither differences in bone and tissue volume nor in bone surface and bone mineral density of callus tissue at these time points (Figure 3B). Histological analysis of non-decalcified cryo-sections of callus tissue confirmed that reboxetine did not interfere with bone regeneration at early and intermediate stages of the healing process (Figure 4A). In particular, quantification of cartilaginous and mineralized components of the callus revealed no significant alterations 7, 14 and 21 days after surgery (Figure 4B). Finally, we assessed the cellular callus parameters 21 days after surgery, as this represents a time point of intense cellular callus remodeling. Osteoclast parameters were not altered, however, mice treated with reboxetine displayed elevated osteoblast numbers and surface (Figures 4C and 4D).

Reboxetine improves late-stage fracture healing

Based on the above observations, we assayed fracture healing 28 days following surgery, corresponding to the late stage of bone healing in mice. μCT scanning demonstrated no significant alteration in bone volume and tissue volume of the fracture callus (Figures 5A and 5B). However, monitoring osseous bridging of fracture ends, we observed improved fracture union in mice receiving reboxetine (Figure 5C). In line with this finding, the biomechanical stability of healed bones was superior in reboxetine-treated mice, as evidenced by an increased maximal force and required work to structural failure (Figure 5D).

Reboxetine induces the expression of osteoblast markers in the early healing stage

To understand this observation on a molecular level, we subjected mice to a femoral osteotomy and extracted callus mRNA 3, 7, and 14 days after surgery. Monitoring the expression of markers for angiogenesis and inflammation, both processes pivotal to bone regeneration, no significant differences were found except for platelet-derived growth factor receptor beta (*Pdgfrb*), whose expression was decreased 7 days following osteotomy (Figures 6A and 6B). Likewise, expression of the osteoclast markers *Calcr* (encoding the calcitonin receptor) and *Ctsk* (encoding cathepsin K) did not differ between reboxetine- and vehicle-treated mice (Figure 6C). In the case of osteoblast parameters, we detected an increased expression of *Alpl* (alkaline phosphatase), *Atf4* (encoding the key osteoblast activating transcription factor 4), *Bglap* (encoding osteocalcin, indicative of osteoblast function), and *Dmp1* (encoding dentin matrix protein 1 involved in matrix mineralization) in the reboxetine group at day 3 following surgery, which normalized during the subsequent course of bone regeneration and were found decreased by tendency at post-operative day 14 (Figure 6D). These indices of enhanced osteogenesis were confirmed by enhanced alkaline phosphatase activity in the callus of mice receiving reboxetine 7 days following osteotomy (Figure S3).

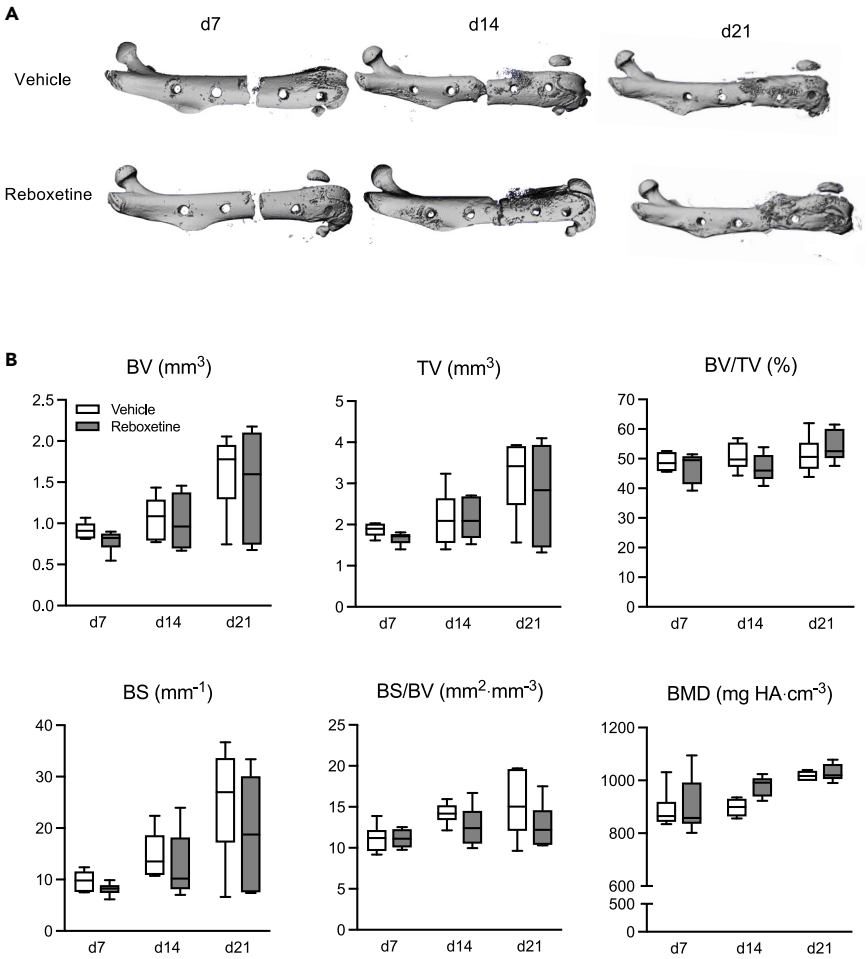

Figure 3. Reboxetine does not impair the early or intermediate stages of fracture healing

(A) Representative μCT images of the healing femur of reboxetine- and vehicle-treated mice 7, 14, and 21 days following fracture.

(B) Quantitative analysis of μCT images in the same mice. BV = total callus bone volume, TV = total tissue volume, BV/TV = bone volume vs. tissue volume, BS = bone surface, BS/BV = bone surface vs. bone volume, BMD = bone mineral density.

n = 6 mice per group. Unpaired Student's *t* test, data are shown in boxplots with median, 25th and 75th quantiles. Whiskers indicate upper and lower extremes, respectively.

DISCUSSION

In the current study, we investigated the impact of systemic treatment with the SNRI reboxetine on bone regeneration in mice. Based on the previously reported, negative impact on bone remodeling with increased bone resorption and decreased bone formation, we hypothesized that reboxetine impairs bone healing, which is of clinical importance in fracture patients prescribed SNRI. Based on the results of this study, our hypothesis was rejected, as reboxetine did not impair early and intermediate healing stages, and even improved long-term regenerative outcomes.

Prior studies using genetic and pharmacological approaches provide solid evidence that beta-adrenergic signaling is a key determinant of bone remodeling. Global and osteoblast genetic ablation of the beta 2 adrenoreceptor results in high trabecular bone mass, as bone formation is enhanced, and bone resorption reduced.[15] These findings underline the importance of sympathetic innervation of bone tissue and neuronal control of bone cell activity. A previous study elegantly showed that osteoblasts express NET and are capable of NE uptake and degradation, thus contributing significantly to the delicate homeostasis of NE signaling in the skeleton.[9] The authors also showed that both pharmacologic inhibition via reboxetine, or genetic inactivation of NET, resulted in decreased trabecular bone mass. While these effects were observed in both spine and femur of male mice, trabecular bone loss exclusively in the axial skeleton, but not long bones, was observed in the case of female animals in the respective study.

In our current study, we employed only female mice to investigate the effect of reboxetine on bone regeneration. In concordance with the previous study by Ma et al., we observed a decreased trabecular bone volume in the spine, but not femur, after 21 days of systemic reboxetine treatment, indicating effective administration of reboxetine. In the spine, this effect was accompanied by an increase in osteoclast

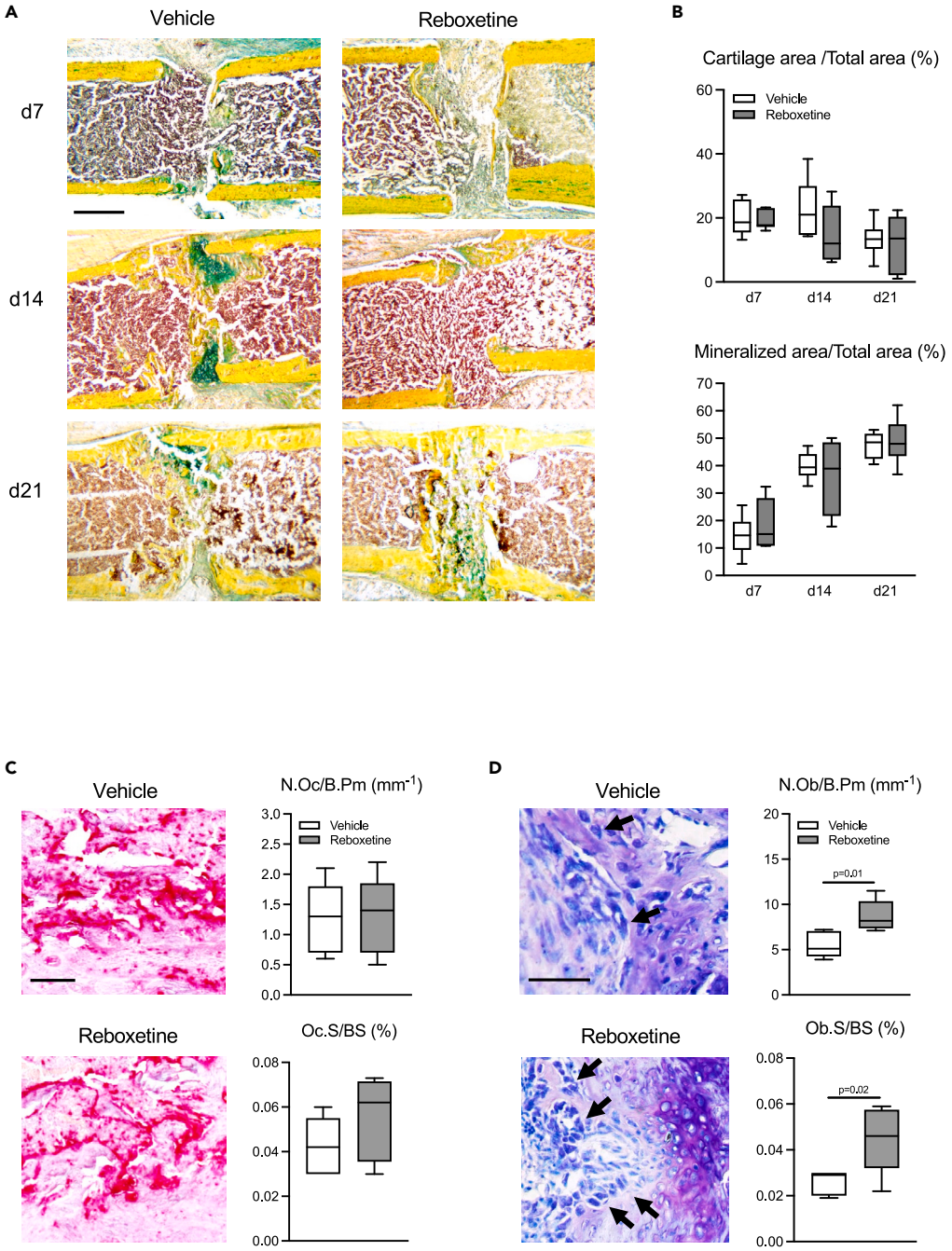

Figure 4. Reboxetine is associated with increased cellular indices of bone formation in the fracture callus

(A) Representative callus sections (Movat's Pentachrome staining) of reboxetine- and vehicle-treated mice at the indicated time points (yellow = mineralized bone; green = cartilage; reddish/brown = bone marrow). Scale bar = 500 μm.

(B) Histomorphometric quantification of static callus parameters (cartilage and mineralized area per total area) in the same mice. The different timepoints were evaluated independently and compared by unpaired Student's *t* test.

(C) Representative callus images and histomorphometric measurement of osteoclast parameters in TRAP-stained callus sections in reboxetine- and vehicle-treated mice 21 days following the femoral osteotomy. Scale bar = 50 μm.

(D) Representative images and histomorphometric assessment of osteoblast numbers and surface in toluidine blue-stained callus sections. Osteoblasts are indicated by black arrows. Scale bar = 25 μm. n = 6 mice per group. Unpaired Student's *t* test, data are shown in boxplots with median, 25th and 75th quantiles. Whiskers indicate upper and lower extremes, respectively.

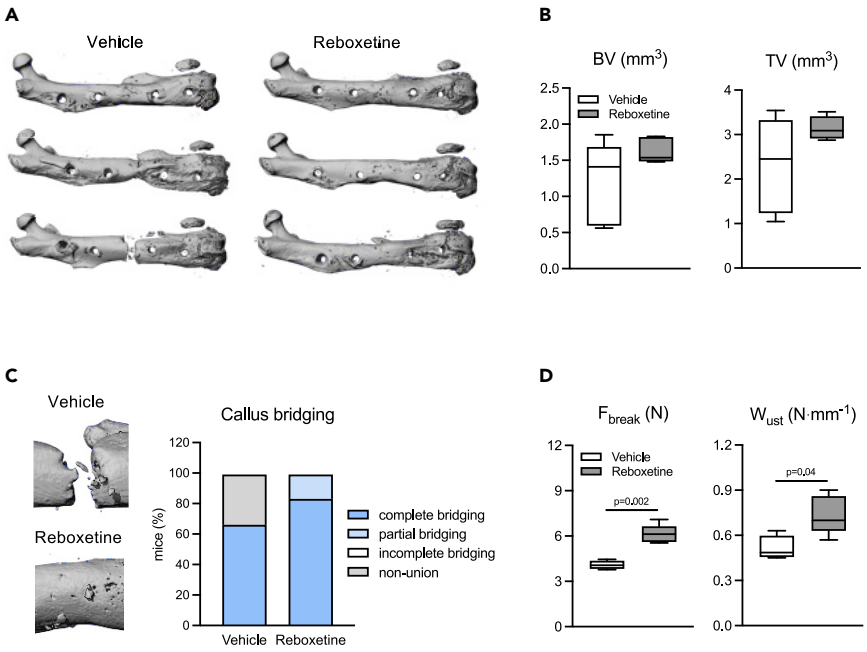

Figure 5. Reboxetine improves late-stage fracture healing

(A and B) (A) Representative μCT images of the healing femur of reboxetine- and vehicle-treated mice 28 days after osteotomy and (B) radiologic assessment of structural callus parameters (BV = bone volume; TV = tissue volume).

(C) Exemplary callus images (μCT images) representing complete union (top) or non-union (bottom), and semiquantitative evaluation of osseous callus bridging in reboxetine- and vehicle-treated mice 28 days after osteotomy: complete bridging = all four cortices bridged by callus, partial bridging = two to three cortices bridged by callus, incomplete bridging = callus present, but no bridging visible, and non-union = rounded cortices, minimal presence of callus.

(D) Quantification of mechanical properties of the healing femora as determined by 3-point bending in the same animals. F_{break} = maximum force that the bone could withstand; W_{uts} = work to ultimate tensile strength. n = 6 mice per group. Unpaired Student's *t* test, data are shown in boxplots with median, 25th and 75th quantiles. Whiskers indicate upper and lower extremes, respectively.

parameters, while trabecular bone cell parameters in the distal femur remained unaltered. In the midshaft area of the femur, reboxetine did not change indices of cortical bone resorption including cortical porosity and osteoclast numbers. However, we found reboxetine to increase the cortical thickness of the femur, which was accompanied by elevated osteoblast numbers. This contrasts with the study by Ma et al. and is possibly explained by the fact that the authors employed continuous release of reboxetine, while our study relied on daily injections. Also, it is possible that the fracture itself primes the non-fractured skeleton to a different response to NET inhibition, as Ma et al. studied mice without fractures. Together, these observations, however, indicate that during fracture healing reboxetine treatment once daily exerts a site-specific effect on bone remodeling in the non-fractured skeleton, with catabolic action in trabecular bone and anabolic impact on cortical bone. This is of special clinical relevance, as total disruption and subsequent healing of cortical bone is central to any skeletal fracture.

Although expression of NET, the principal target of reboxetine, was previously demonstrated in osteoblasts, trabecular and cortical bone, a possible role in bone regeneration was unknown. We thus analyzed NET expression in the callus during fracture healing, where we observed a progressive and striking induction of NET following a femoral osteotomy. As periosteal cells migrate into the site of skeletal injury and differentiate into bone-forming osteoblasts, we also monitored NET expression in periosteal cells generated *ex vivo*. Here, NET expression also progressively increased during osteogenic differentiation of periosteal cells, suggesting a functional relevance during long bone healing. During the early and intermediate healing phases (i.e., post-operative day 7–21), reboxetine did not affect any static radiologic and histologic outcome measurements. However, in line with the increased osteoblast numbers in the cortical bone of the contralateral non-fractured femur, reboxetine treatment was associated with increased osteoblast parameters in the callus 21 days following the osteotomy. This finding translated into improved osseous callus bridging and improved biomechanical stability in the reboxetine group 28 days after surgery. On a molecular level, while indices of inflammatory responses and osteoclasts were unaffected, an induced expression of the key osteoblast marker genes *Atf4*, *Bglap* and *Dmp1* was detected at day 3 following osteotomy. In this regard, *Atf4* plays master roles in osteoblast proliferation and differentiation by its transcriptional regulation of key genes involved in bone formation, including *Bglap* encoding osteocalcin. Moreover, *Dmp1* represents a major extracellular matrix protein with essential relevance for osteogenesis. These markers were induced at a very early healing stage, subsequently normalized, and even decreased by tendency at later stages, pointing toward an overall accelerated healing course in mice receiving reboxetine. Together, our findings suggest that osteogenesis is enhanced by reboxetine treatment at very early stages on a transcriptional level, resulting in increased cellular osteoblast parameters at intermediate stages and improved healing outcomes at later stages.

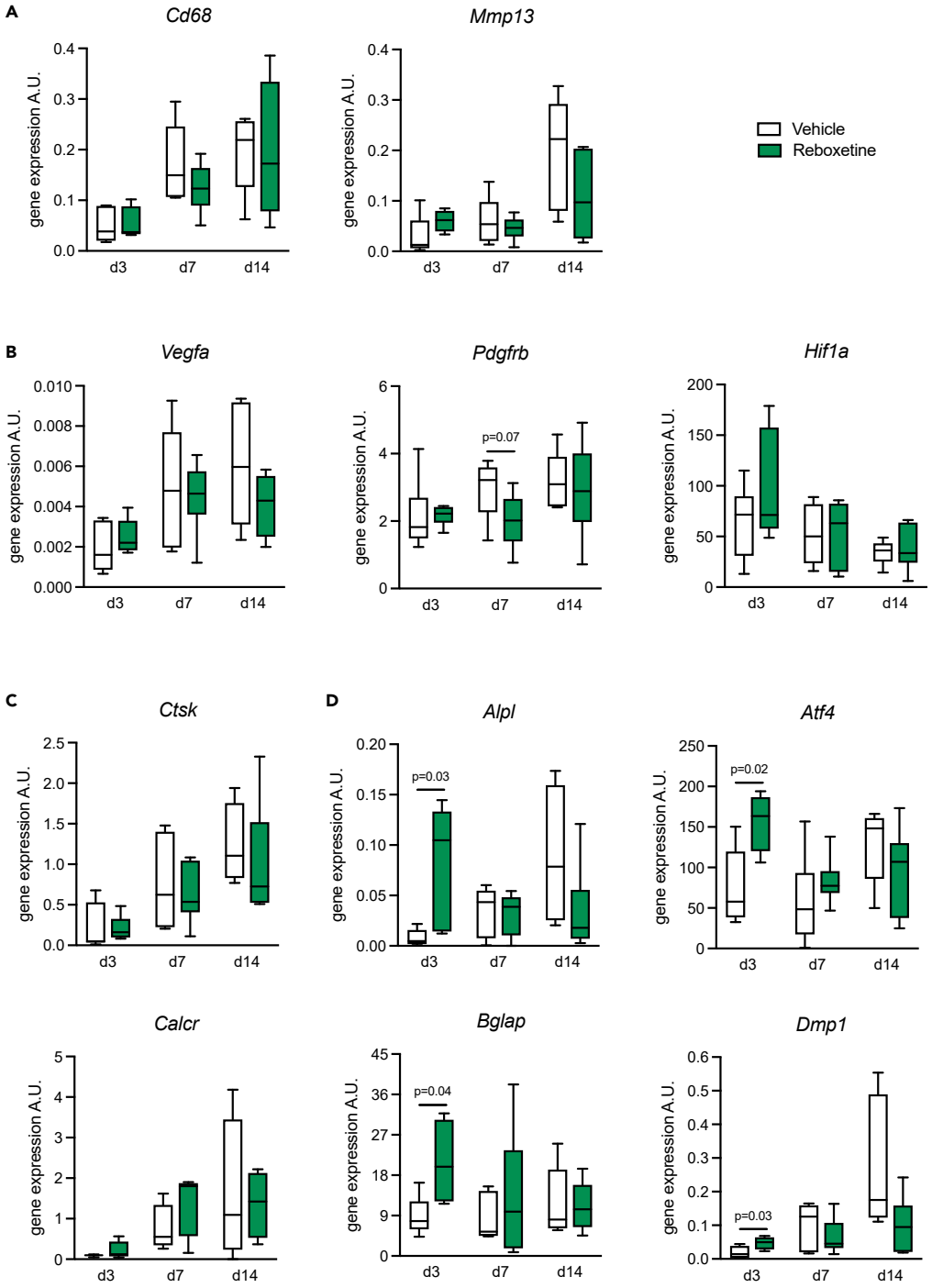

Figure 6. Reboxetine induces the expression of osteoblast markers in the early healing stage

(A–D) qRT-PCR expression analysis (virtual copy numbers per Gapdh; *A.U. = arbitrary units)* of the indicated genes in the callus of reboxetine- or vehicle-treated mice at the indicated time points after osteotomy. *Cd68* = cluster of differentiation 68; *MMP13* = matrix metalloproteinase 13; *Vegfa* = vascular endothelial growth factor A; *Pdgfrb* = platelet-derived growth factor receptor beta; *Hif1α* = hypoxia inducible factor 1 subunit alpha; *Ctsk* = cathepsin K; *Calcr* = calcitonin receptor; *Alpl* = alkaline phosphatase; *Atf4* = activating transcription factor 4; *Bglap* = bone gla protein, alternatively termed osteocalcin; *Dmp1* = dentin matrix protein 1. n = 6 mice per group. Non-parametric Mann–Whitney U test, data are shown in boxplots with median, 25th and 75th quantiles. Whiskers indicate upper and lower extremes, respectively.

To the best of our knowledge, no clinical data describing the effects of SNRI on fracture healing is currently available. Over the last decades, various studies provided evidence for increased fracture risk upon use of SNRI. A nationwide Chinese case-control study reported an adjusted odds ratio of 1.16 for fracture risk in SNRI users.[16] Furthermore, an adjusted hazard ratio of 1.68 for fracture risk in patients using SNRI was observed in a prospective Canadian trial.[13] In comparison with other antidepressant drugs, such as selective serotonin reuptake inhibitors (SSRI), a retrospective US-American trial showed that fracture risk in patients using SNRI is elevated by tendency.[17] There are several factors contributing to the observed adverse effects concerning the musculoskeletal system. Generally, comorbidities such as a history of falling and osteoporosis are frequent in SNRI users and increase fracture risk independently, as summarized recently in a meta-analysis by Sobieraj et al.[18] In addition, administration of SNRI was reported to lower bone mass at various sites of the skeleton. Results of a population-based cohort study show significantly decreased radial T-scores and a reduction of cortical tibial BMD by −4% upon SNRI use; however, disuse bone wasting due to accompanying reduced physical function in studied elderly women could not be excluded.[19] In line with these findings, however, increased bone resorption activity, as indicated by elevation of serum β-CTX levels, has overall been observed in patients using SNRI.[20] Thus, although currently available evidence is suggesting an increased fracture risk due to enhanced bone resorption associated with SNRI use, further clinical studies are warranted to also examine its impact on bone healing.

In conclusion, our study shows that reboxetine exerts site-specific effects in the non-fractured skeleton, with anabolic action in femoral cortical bone. Furthermore, our results demonstrate that a systemic, pharmacologic inhibition of NET does not impair femoral bone healing at early and intermediate healing stages in mice, and even results in improved healing outcomes at late stages. Although caution must be taken when translating these findings into the clinical situation, our data imply that patients taking SNRI are not at risk for impaired fracture healing. Contrary to the current understanding of NE as a catabolic mediator in bone, our study results indicate that NE signaling can exert anabolic actions on the fractured and non-fractured skeleton in a context dependent manner.

Limitations of the study

Our study has several limitations. First, we only employed female mice to allow better comparability with similar studies investigating bone remodeling and regeneration. Thus, it is possible that male mice respond differently to reboxetine treatment during fracture healing. Second, we cannot define to which degree NET inhibition occurred with the chosen pharmacologic approach, as we did not determine systemic or local NE levels within the fracture callus. Yet, based on the observed skeletal effects in non-fractured, trabecular bone, which are similar to that of Ma et al., we conclude that NE inhibition by reboxetine was effective in our chosen model. Third, to allow better comparability with previous studies, mice received the osteotomy at the age of 12–14 weeks, and reboxetine treatment was initiated at the time of surgery. Administration of SNRIs before this age, especially in female mice, would be similar to administration of SNRIs in adolescents, who have a different metabolism of neurotransmitters, including NA, extremely high neuronal plasticity, and premature anatomical structures that are still subject to change.[21–23] And finally, our study does not allow formal conclusions regarding the underlying mechanisms by which reboxetine improves late-stage bone healing. In this regard, systemic application of the SNRI reboxetine results in global inhibition of NET, which is expressed in a broad array of different cell types and organ systems involved in bone repair.[24,25] Inhibition of NET may also affect the signal transduction activities of alpha- and beta-adrenergic cell surface receptors with significant impact on bone cell differentiation and function. Although our data clearly suggest a pro-osteogenic effect of reboxetine during bone regeneration, future studies using cell-type specific NET inactivation are thus warranted to explain how the contrasting impact of reboxetine in trabecular and cortical bone is explained on a mechanistic level, and how this translates into improved late-stage bone healing.

STAR★METHODS

Detailed methods are provided in the online version of this paper and include the following:

- KEY RESOURCES TABLE
- RESOURCE AVAILABILITY
  - Lead contact
  - Materials availability
  - Data and code availability
- EXPERIMENTAL MODEL AND STUDY PARTICIPANT DETAILS
  - Animal experiments
  - Materials
  - Surgery and treatment
- METHOD DETAILS
  - Micro-computed tomography
  - Histomorphometry of the callus
  - Histomorphometry of the spine and intact femur
  - Biomechanics
  - Periosteal cell culture

- RNA extraction and qRT-PCR
- ELISA

- QUANTIFICATION AND STATISTICAL ANALYSIS

SUPPLEMENTAL INFORMATION

Supplemental information can be found online at https://doi.org/10.1016/j.isci.2023.107761.

ACKNOWLEDGMENTS

We would like to thank Ms. Cordula Erdmann, Ms. Saskia Schröder and Ms. Mayla Rickert for skillful technical assistance. Graphical abstract and Figure 1C were created with Biorender.com. This work was supported by the German Research Foundation [grant numbers KE 2179/2-3 and TS 303/2-3].

AUTHOR CONTRIBUTIONS

A.D. performed experiments, collected and interpreted the data, and edited the manuscript. S.J. and W.X. contributed to surgery, data analysis, and tissue sampling. P.R.K., L-C.A., J.L.K., J.S., and R.A. assisted with surgery and tissue sampling. T.A.Y. performed biomechanical testing. D.J. and S.T. provided critical discussion. A.B. designed and supervised the study and interpreted the data. J.K. designed and supervised the study, interpreted the data, and wrote the manuscript. All authors approved the final version of the manuscript.

DECLARATION OF INTERESTS

J.K. and S.T. disclose support for the research of this work from the German Research Foundation [grant numbers KE 2179/2-3 and TS 303/2-3].

Received: April 18, 2023
Revised: August 3, 2023
Accepted: August 25, 2023
Published: August 29, 2023

REFERENCES

1. Westgeest, J., Weber, D., Dulai, S.K., Bergman, J.W., Buckley, R., and Beaupre, L.A. (2016). Factors Associated With Development of Nonunion or Delayed Healing After an Open Long Bone Fracture: A Prospective Cohort Study of 736 Subjects. J. Orthop. Trauma *30*, 149–155. https://doi.org/10.1097/bot.0000000000000488.
2. Goudie, E.B., and Robinson, C.M. (2021). Prediction of Nonunion After Nonoperative Treatment of a Proximal Humeral Fracture. J. Bone Joint Surg. Am. *103*, 668–680. https://doi.org/10.2106/jbjs.20.01139.
3. Hak, D.J., Fitzpatrick, D., Bishop, J.A., Marsh, J.L., Tilp, S., Schnettler, R., Simpson, H., and Alt, V. (2014). Delayed union and nonunions: epidemiology, clinical issues, and financial aspects. Injury *45*, S3. https://doi.org/10.1016/j.injury.2014.04.002.
4. Wichlas, F., Tsitsilonis, S., Disch, A.C., Haas, N.P., Hartmann, C., Graef, F., and Schwabe, P. (2015). Long-term functional outcome and quality of life after successful surgical treatment of tibial nonunions. Int. Orthop. *39*, 521–525. https://doi.org/10.1007/s00264-014-2629-y.
5. Tanaka, K., Hirai, T., Kodama, D., Kondo, H., Hamamura, K., and Togari, A. (2016). α1B -Adrenoceptor signalling regulates bone formation through the up-regulation of CCAAT/enhancer-binding protein δ expression in osteoblasts. Br. J. Pharmacol. *173*, 1058–1069. https://doi.org/10.1111/bph.13418.
6. Ferroni, L., Gardin, C., Bellin, G., Vindigni, V., Pavan, C., and Zavan, B. (2019). Effects of novel antidepressant drugs on mesenchymal stem cell physiology. Biomed. Pharmacother. *114*, 108853. https://doi.org/10.1016/j.biopha.2019.108853.
7. Aitken, S.J., Landao-Bassonga, E., Ralston, S.H., and Idris, A.I. (2009). Beta2-adrenoreceptor ligands regulate osteoclast differentiation *in vitro* by direct and indirect mechanisms. Arch. Biochem. Biophys. *482*, 96–103. https://doi.org/10.1016/j.abb.2008.11.012.
8. Zhu, Y., Ma, Y., and Elefteriou, F. (2018). Cortical bone is an extraneuronal site of norepinephrine uptake in adult mice. Bone Rep. *9*, 188–198. https://doi.org/10.1016/j.bonr.2018.11.002.
9. Ma, Y., Krueger, J.J., Redmon, S.N., Uppuganti, S., Nyman, J.S., Hahn, M.K., and Elefteriou, F. (2013). Extracellular norepinephrine clearance by the norepinephrine transporter is required for skeletal homeostasis. J. Biol. Chem. *288*, 30105–30113. https://doi.org/10.1074/jbc.M113.481309.
10. Sáiz-Ruiz, J., Ibáñez, A., Díaz-Marsá, M., Arias, F., Padín, J., Martín-Carrasco, M., Montes, J.M., Ferrando, L., Carrasco, J.L., Martín-Ballesteros, E., et al. (2002). Efficacy of venlafaxine in major depression resistant to selective serotonin reuptake inhibitors. Prog. Neuro-Psychopharmacol. Biol. Psychiatry *26*, 1129–1134. https://doi.org/10.1016/s0278-5846(02)00247-6.
11. Hollander, E., Friedberg, J., Wasserman, S., Allen, A., Birnbaum, M., and Koran, L.M. (2003). Venlafaxine in treatment-resistant obsessive-compulsive disorder. J. Clin. Psychiatry *64*, 546–550. https://doi.org/10.4088/jcp.v64n0508.
12. Chamberlain, S.R., Del Campo, N., Dowson, J., Müller, U., Clark, L., Robbins, T.W., and Sahakian, B.J. (2007). Atomoxetine improved response inhibition in adults with attention deficit/hyperactivity disorder. Biol. Psychiatry *62*, 977–984. https://doi.org/10.1016/j.biopsych.2007.03.003.
13. Moura, C., Bernatsky, S., Abrahamowicz, M., Papaioannou, A., Bessette, L., Adachi, J., Goltzman, D., Prior, J., Kreiger, N., Towheed, T., et al. (2014). Antidepressant use and 10-year incident fracture risk: the population-based Canadian Multicentre Osteoporosis Study (CaMoS). Osteoporos. Int. *25*, 1473–1481. https://doi.org/10.1007/s00198-014-2649-x.
14. Bakken, M.S., Engeland, A., Engesæter, L.B., Ranhoff, A.H., Hunskaar, S., and Ruths, S. (2013). Increased risk of hip fracture among older people using antidepressant drugs: data from the Norwegian Prescription Database and the Norwegian Hip Fracture Registry. Age Ageing *42*, 514–520. https://doi.org/10.1093/ageing/aft009.
15. Pierroz, D.D., Bonnet, N., Bianchi, E.N., Bouxsein, M.L., Baldock, P.A., Rizzoli, R., and Ferrari, S.L. (2012). Deletion of β-adrenergic receptor 1, 2, or both leads to different bone phenotypes and response to mechanical stimulation. J. Bone Miner. Res. *27*, 1252–1262. https://doi.org/10.1002/jbmr.1594.
16. Wang, C.Y., Fu, S.H., Wang, C.L., Chen, P.J., Wu, F.L.L., and Hsiao, F.Y. (2016). Serotonergic antidepressant use and the risk of fracture: a population-based nested

case-control study. Osteoporos. Int. *27*, 57–63. https://doi.org/10.1007/s00198-015-3213-z.

17. Lanteigne, A., Sheu, Y.H., Stürmer, T., Pate, V., Azrael, D., Swanson, S.A., and Miller, M. (2015). Serotonin-norepinephrine reuptake inhibitor and selective serotonin reuptake inhibitor use and risk of fractures: a new-user cohort study among US adults aged 50 years and older. CNS Drugs *29*, 245–252. https://doi.org/10.1007/s40263-015-0231-5.
18. Sobieraj, D.M., Martinez, B.K., Hernandez, A.V., Coleman, C.I., Ross, J.S., Berg, K.M., Steffens, D.C., and Baker, W.L. (2019). Adverse Effects of Pharmacologic Treatments of Major Depression in Older Adults. J. Am. Geriatr. Soc. *67*, 1571–1581. https://doi.org/10.1111/jgs.15966.
19. Agarwal, S., Germosen, C., Kil, N., Bucovsky, M., Colon, I., Williams, J., Shane, E., and Walker, M.D. (2020). Current anti-depressant use is associated with cortical bone deficits and reduced physical function in elderly women. Bone *140*, 115552. https://doi.org/10.1016/j.bone.2020.115552.
20. Shea, M.L.O., Garfield, L.D., Teitelbaum, S., Civitelli, R., Mulsant, B.H., Reynolds, C.F., 3rd, Dixon, D., Doré, P., and Lenze, E.J. (2013). Serotonin-norepinephrine reuptake inhibitor therapy in late-life depression is associated with increased marker of bone resorption. Osteoporos. Int. *24*, 1741–1749. https://doi.org/10.1007/s00198-012-2170-z.
21. Murrin, L.C., Sanders, J.D., and Bylund, D.B. (2007). Comparison of the maturation of the adrenergic and serotonergic neurotransmitter systems in the brain: implications for differential drug effects on juveniles and adults. Biochem. Pharmacol. *73*, 1225–1236. https://doi.org/10.1016/j.bcp.2007.01.028.
22. Sanders, J.D., Happe, H.K., Bylund, D.B., and Murrin, L.C. (2011). Changes in postnatal norepinephrine alter alpha-2 adrenergic receptor development. Neuroscience *192*, 761–772. https://doi.org/10.1016/j.neuroscience.2011.06.045.
23. Bradshaw, S.E., Agster, K.L., Waterhouse, B.D., and McGaughy, J.A. (2016). Age-related changes in prefrontal norepinephrine transporter density: The basis for improved cognitive flexibility after low doses of atomoxetine in adolescent rats. Brain Res. *1641*, 245–257. https://doi.org/10.1016/j.brainres.2016.01.001.
24. Wong, E.H., Sonders, M.S., Amara, S.G., Tinholt, P.M., Piercey, M.F., Hoffmann, W.P., Hyslop, D.K., Franklin, S., Porsolt, R.D., Bonsignori, A., et al. (2000). Reboxetine: a pharmacologically potent, selective, and specific norepinephrine reuptake inhibitor. Biol. Psychiatry *47*, 818–829. https://doi.org/10.1016/s0006-3223(99)00291-7.
25. Ayala-Lopez, N., and Watts, S.W. (2021). Physiology and Pharmacology of Neurotransmitter Transporters. Compr. Physiol. *11*, 2279–2295. https://doi.org/10.1002/cphy.c200035.
26. Jiang, S., Knapstein, P., Donat, A., Tsitsilonis, S., and Keller, J. (2021). An optimized protocol for a standardized, femoral osteotomy model to study fracture healing in mice. STAR Protoc. *2*, 100798. https://doi.org/10.1016/j.xpro.2021.100798.
27. Dziedzicka-Wasylewska, M., Faron-Górecka, A., Kuśmider, M., Drozdowska, E., Rogóz, Z., Siwanowicz, J., Caron, M.G., and Bönisch, H. (2006). Effect of antidepressant drugs in mice lacking the norepinephrine transporter. Neuropsychopharmacology *31*, 2424–2432. https://doi.org/10.1038/sj.npp.1301064.
28. Cryan, J.F., O'Leary, O.F., Jin, S.H., Friedland, J.C., Ouyang, M., Hirsch, B.R., Page, M.E., Dalvi, A., Thomas, S.A., and Lucki, I. (2004). Norepinephrine-deficient mice lack responses to antidepressant drugs, including selective serotonin reuptake inhibitors. Proc. Natl. Acad. Sci. USA *101*, 8186–8191. https://doi.org/10.1073/pnas.0401080101.
29. Bouxsein, M.L., Boyd, S.K., Christiansen, B.A., Guldberg, R.E., Jepsen, K.J., and Müller, R. (2010). Guidelines for assessment of bone microstructure in rodents using micro-computed tomography. J. Bone Miner. Res. *25*, 1468–1486. https://doi.org/10.1002/jbmr.141.
30. Kawamoto, T., and Kawamoto, K. (2014). Preparation of thin frozen sections from nonfixed and undecalcified hard tissues using Kawamot's film method (2012). Methods Mol. Biol. *1130*, 149–164. https://doi.org/10.1007/978-1-62703-989-5_11.
31. Appelt, J., Tsitsilonis, S., Otto, E., Jahn, D., Köhli, P., Baranowsky, A., Jiang, S., Fuchs, M., Bucher, C.H., Duda, G.N., et al. (2021). Mice Lacking the Calcitonin Receptor Do Not Display Improved Bone Healing. Cells *10*, 2304. https://doi.org/10.3390/cells10092304.
32. Miao, D., and Scutt, A. (2002). Histochemical localization of alkaline phosphatase activity in decalcified bone and cartilage. J. Histochem. Cytochem. *50*, 333–340. https://doi.org/10.1177/002215540205000305.
33. Schinke, T., Schilling, A.F., Baranowsky, A., Seitz, S., Marshall, R.P., Linn, T., Blaeker, M., Huebner, A.K., Schulz, A., Simon, R., et al. (2009). Impaired gastric acidification negatively affects calcium homeostasis and bone mass. Nat. Med. *15*, 674–681. https://doi.org/10.1038/nm.1963.
34. Hahn, M., Vogel, M., and Delling, G. (1991). Undecalcified preparation of bone tissue: report of technical experience and development of new methods. Virchows Arch. A Pathol. Anat. Histopathol. *418*, 1–7. https://doi.org/10.1007/bf01600238.
35. Keller, J., Catala-Lehnen, P., Huebner, A.K., Jeschke, A., Heckt, T., Lueth, A., Krause, M., Koehne, T., Albers, J., Schulze, J., et al. (2014). Calcitonin controls bone formation by inhibiting the release of sphingosine 1-phosphate from osteoclasts. Nat. Commun. *5*, 5215. https://doi.org/10.1038/ncomms6215.
36. Dempster, D.W., Compston, J.E., Drezner, M.K., Glorieux, F.H., Kanis, J.A., Malluche, H., Meunier, P.J., Ott, S.M., Recker, R.R., and Parfitt, A.M. (2013). Standardized nomenclature, symbols, and units for bone histomorphometry: a 2012 update of the report of the ASBMR Histomorphometry Nomenclature Committee. J. Bone Miner. Res. *28*, 2–17. https://doi.org/10.1002/jbmr.1805.
37. Parfitt, A.M., Drezner, M.K., Glorieux, F.H., Kanis, J.A., Malluche, H., Meunier, P.J., Ott, S.M., and Recker, R.R. (1987). Bone histomorphometry: standardization of nomenclature, symbols, and units. Report of the ASBMR Histomorphometry Nomenclature Committee. J. Bone Miner. Res. *2*, 595–610. https://doi.org/10.1002/jbmr.5650020617.
38. Savi, F.M., Lawrence, F., Hutmacher, D.W., Woodruff, M.A., Bray, L.J., and Wille, M.L. (2019). Histomorphometric Evaluation of Critical-Sized Bone Defects Using Osteomeasure and Aperio Image Analysis Systems. Tissue Eng. Part C Methods *25*, 732–741. https://doi.org/10.1089/ten.TEC.2019.0179.
39. Luther, J., Yorgan, T.A., Rolvien, T., Ulsamer, L., Koehne, T., Liao, N., Keller, D., Vollersen, N., Teufel, S., Neven, M., et al. (2018). Wnt1 is an Lrp5-independent bone-anabolic Wnt ligand. Sci. Transl. Med. *10*, eaau7137. https://doi.org/10.1126/scitranslmed.aau7137.

STAR★METHODS

KEY RESOURCES TABLE

REAGENT or RESOURCE	SOURCE	IDENTIFIER
Chemicals, peptides, and recombinant proteins		
Reboxetine mesylate	AdooQ BioScience	Cat#A11919; CAS: 98769-84-7
Clindamycin	Hikma Pharma	Cat#42482.01.00
Burprenorphine	Richter Pharma	Cvet code: QN02AE01
Metamizole	Ratiopharm	PZN 03530394; EAN 4150035303945
Critical commercial assays		
NucleoSpin RNA Kit	Macherey-Nagel	Cat#740955.50
ProtoScript First Strand cDNA Synthesis Kit	New England BioLabs	Cat#E6300L
Norepinephrine High Sensitive ELISA	Immusmol	Cat#BA-E-5200R
Experimental models: Organisms/strains		
C57BL/6J mice	The Jackson Laboratory	Cat#000664
Oligonucleotides		
Primers for SYBR Green: *Gapdh* (FOR-TGCACCAACTGCTTAG, REV-GGATGCAGGGATGATGTTC) *Pdgfrb* (FOR-AGTGAGGACAGACGTCCCAT, REV-GAGGTGGTAATCCCGTCAGC) *Slc6a2* (FOR-TGTGTTTGTACGCCCAGGTG, REV-ACCTCCTAGCACCTTCGTGA)	This paper	N/A
TaqMan Primer (*Alpl, Atf4, Bglap, Calcr, Cd68, Ctsk, Dmp1, Gapdh, Hif1a, MMP13, Ucp1*)	ThermoFischer	Cat#4331182; Assay-IDs available in manuscript
Software and algorithms		
GraphPad PRISM	Graphpad Software, Inc.	N/A
ImageJ Analysis System	NIH	https://imagej.net/ij/index.html
OsteoMeasure	Osteometrics Inc.	N/A
Other		
MouseExFix simple	RISystem	Cat#RIS.611.200
MouseExFix Mounting Pin 0.45 mm	RISystem	Cat#RIS.411.100
Square box wrench 0.70 mm	RISystem	Cat#RIS.590.112
Drill bit 0.45 mm	RISystem	Cat#RIS.590.201
Gigli wire saw 0.7mm	RISystem	Cat#RIS.590.120-25
Hand drill	RISystem	Cat#RIS.390.XXX
Mersilene	Ethicon	Cat#eh7147h

RESOURCE AVAILABILITY

Lead contact

Further information and requests concerning resources and reagents should be directed to and will be answered by the lead contact, Prof. Dr. Dr. Johannes Keller (j.keller@uke.de).

Materials availability

This study did not generate new unique reagents.

Data and code availability

- All relevant data of this project is presented within the figures of this manuscript. Research raw data associated with this manuscript will be shared by the lead contact upon reasonable request.
- This paper does not report original code.
- Any additional information required to reanalyze the data reported in this paper is available from the lead contact upon request.

EXPERIMENTAL MODEL AND STUDY PARTICIPANT DETAILS

Animal experiments

Female wild-type (WT) mice with a C57Bl/6J genetic background and body weight > 20 g were used for the study. All experiments were carried out according to the international directives on the protection of laboratory animals (Directive 2010/63/EU) and are in line with the ARRIVE guidelines for animal studies. The study was approved by animal facility of the University Hospital Hamburg-Eppendorf and the local animal welfare authorities (No. N124/2020, Behörde für Justiz und Verbraucherschutz, Freie und Hansestadt Hamburg, Germany) prior to project start. Animals were maintained under standard conditions (12 h light-dark circadian rhythm, 22°C room temperature) in a SPF facility. They were housed in stable groups of two to three animals per cage. Water and a standard diet were provided *ad libitum*.

Materials

The following substances were used for animal experiments: Reboxetine mesylate (AdooQ BioScience, Irvine, Canada), clindamycin (Hikma Pharma GmbH, Martinsried, Germany), buprenorphine (Buprenovet®, Richter Pharma AG, Wels, Austria), metamizole (Novaminsulfon-ratiopharm®, Ratiopharm, Ulm, Germany).

Surgery and treatment

At the age of 12-14 weeks, the mice received a femoral fracture, stabilized by an external fixator, as previously described.[26] In brief, the mice were anesthetized, and the left femur was exposed. Four pins were drilled with a hand-drill (diameter: 0.45 mm) and a commercially available external fixator (RISystem, Davos, Switzerland) was installed on the femur. The fracture gap was generated using a Gigli wire saw with a diameter of 0.7 mm. Wound closure was accomplished using a simple interrupted suture. Clindamycin (150 $mg \cdot kg^{-1}$) and buprenorphine (0.1 $mg \cdot kg^{-1}$) were administered prior to surgery. For optimal pain relief, metamizole (1 $mg \cdot ml^{-1}$) was administered via the drinking water for 3 days post-operatively. From the timepoint of surgery until sacrification, the mice received daily injections of either vehicle (0.9% saline) or the selective norepinephrine reuptake inhibitor (SNRI) reboxetine at 15 $mg \cdot kg^{-1}$, diluted in 0.9% saline, with a total volume of 100 µl intraperitoneally. The dosage lies within the therapeutic range of 5-20 $mg \cdot kg^{-1}$ and has been used in several previous studies without report of adverse effects.[27,28] Littermates were assigned randomly to experimental groups and sacrificed on post-operative days 3, 7, 14, 21 and 28 by final exsanguination under isoflurane anesthesia and samples were collected subsequently.

METHOD DETAILS

Micro-computed tomography

The fractured and contralateral femur as well as the spine (L1-L4) were scanned using µCT (VivaCT 80, SCANCO Medical AG, Brüttisellen, Switzerland) at voxel resolution of 15.6 µm, 400 ms integration time, 70 kVp and 113 µA. For evaluation of the callus, the volume of interest (VOI) was determined by the cortical composition of the fracture ends and a total of 100 slides was contoured manually. Data is displayed as suggested by the American Society for Bone and Mineral Research guidelines for µCT analysis.[29] For evaluation of the contralateral femur, the whole femur was scanned and a 2 mm long midshaft area as well as a 2 mm long distal segment were calculated accordingly. Cortical and trabecular properties were derived through an automatic image analysis algorithm provided by the manufacturer. For evaluation of the spine, a total of four vertebrae were scanned, the trabecular bone of the two middle vertebra bodies was analyzed semi-automatically and the mean values were calculated. On each anatomical site, a consistent threshold was used. For the assessment of late-stage callus bridging, fractured femurs were collected at day 28 after surgery and underwent fixation with 4% paraformaldehyde at 4°C for 24 h. Afterwards, the fixators were removed, and the bones were stored in PBS during µCT scanning. Callus bridging of these samples was evaluated by two blinded researchers on three-dimensional images and categorized with the following scoring system: complete bridging = all four cortices bridged by callus, partial bridging = two or three cortices bridged by callus, incomplete bridging = callus present, but no bridging visible, and non-union = rounded cortices, minimal presence of callus.

Histomorphometry of the callus

Whole femurs were dissected on day 7, 14 and 21 after surgery and fixed with 4% paraformaldehyde at 4°C. After 24 h, the femurs were washed with PBS three times for an hour each. Subsequently, the fixators were removed carefully, and the bones were scanned using µCT. After incubation in an ascending sugar gradient (10%, 20% and 30% each for 24 h at 4°C), the samples were embedded in SCEM medium (Section Lab Co Ltd., Hiroshima, Japan), frozen in hexane (Carl Roth GmbH&CoKG, Karlsruhe, Germany) and stored at -80°C until further processing. Using a cryostat (Leica CM3050S, Leica Microsystems, Nussloch, Germany) with a microtome blade for hard tissue sectioning (Type N35HR, FEATHER Safety Razor Co., Osaka, Japan), longitudinal sections of 7 µm were derived and mounted onto microscope slides

using cryofilm (Cryofilm type II C, Section Lab Co Ltd., Hiroshima, Japan) as described by Kawamoto and Kawamoto in 2014.[30] Stained was performed subsequently, employing either Movat's Pentachrome protocol to estimate the ratio of cartilage and mineralized area or histochemical detection of Alpl activity using Naphthol (Naphthol AS-MX phosphate disodium salt, Sigma Aldrich, Merck, Darmstadt, Germany). Staining with Movat's Pentachrome was performed as described elsewhere.[31] The distribution of cartilage and mineralization within the callus area was calculated semi-automatically using image analysis software (ImageJ Analysis System, NIH, Bethesda, MD, USA). For alkaline phosphatase (Alpl) activity staining, cryo-sections were defrosted and washed with tris buffer (0,1M tris maleate buffer at pH 9.2 with 1% magnesium chloride) at room temperature two times for 5 minutes each. Staining with Naphthol was performed as previously described[32] and coverslips mounted with glycerin gelantine (Carl Roth GmbH&CoKG, Karlsruhe, Germany). Signal intensities in the ROI of the healing fracture (1 mm x 2 mm square placed centrally over the fracture gap) were quantified by two blinded investigators using ImageJ Analysis System (NIH, Bethesda, MD, USA).

Histomorphometry of the spine and intact femur

After fixation of the whole skeleton in 4% formaldehyde for 48 h, vertebra bodies L1-L4 and the contralateral, non-fractured femur were dissected, dehydrated, and embedded undecalcified in methylmetacrylate as previously described.[33] 4 μm sections of the spine and the femur, respectively, were cut using a Microtec rotation microtome. Toluidine blue, von Kossa/van Gieson and TRAP staining was performed as described elsewhere.[34,35] In line with ASMBR recommendations,[36,37] osteoclast numbers per bone surface and osteoclast surface were evaluated by counting TRAP-positive, multinucleated cells on the bone surface on the respective slides. Osteoblast numbers per bone surface and osteoblast surface were evaluated by counting grouped cuboidal cells, located along the bone surface, on Toluidine blue stained sections. Osteocyte numbers per bone area were evaluated by counting bone cells embedded in ellipsoidal cavities within the collagenous extracellular matrix on Toluidine blue stained sections. In addition, manual delineation of the bone surface was performed on the same sections using the OsteoMeasure histomorphometry system (Osteometrics Inc., Atlanta, USA) with 20-fold magnification and manual, region-based selection mode.[38] Subsequently, static and dynamic parameters were calculated semi-automatically by the software on a field-by-field summary basis.

Biomechanics

Following μCT evaluation, all bones harvested on day 28 were challenged with a destructive three-point bending test as previously described.[39] In short, femurs were placed on two support bars of the device (ZwickRoell, Ulm, Germany) and a bending load with a maximum of 20 N was applied medially onto the callus site. Derived parameters were calculated automatically by the software.

Periosteal cell culture

Femurs of euthanized C57Bl/6J WT mice of both genders were harvested at the age of 12-20 weeks, cut open and flushed out several times to remove bone (osteoblasts, osteoclasts) and bone marrow cells. Digestion of periosteal tissue was then induced by incubation with 0.1% dispase (Roche Diagnostics GmbH, Darmstadt, Germany) and 0.25% collagenase II (gibco Life Technologies Corporation, Grand Island, USA) at 37°C for 3 h. Periosteal cells were separated using a 70 μm cell strainer and centrifugation at 1000 RPM for 10 minutes. Subsequently, cells were counted manually and plated onto a 12-well plate in a concentration of 1×10^4 cells per well. α-MEM (Merck KGaA, Darmstadt, Germany) supplemented with 10% FCS was used for cultivation and changed every 2-3 days. Osteogenic differentiation was induced with 25 $\mu g \cdot mL^{-1}$ ascorbic acid and 5 $mmol \cdot L^{-1}$ β-glycerophosphate. On day 0, 4, 9, 15 and 22 after induction of differentiation, cells were lysed in TRIzol (TRI Reagent, Sigma Aldrich, Merck, Darmstadt, Germany) and RNA isolation and gene expression analysis was carried out as described below.

RNA extraction and qRT-PCR

The callus, including both fracture ends, was extracted between the two central pins at day 3, 7 and 14 after surgery. Concomitantly, midshaft femoral sections of an independent group of WT mice (C57Bl/6J genetic background, n = 6 females, 14 weeks old) were dissected 3 days following sham surgery and served as controls (intact bone; data exclusively displayed in Figure 1A). Following snap freezing in liquid nitrogen, further processing was carried out using a standardized purification protocol employing homogenization in TRIzol (Sigma Aldrich, Merck, Darmstadt, Germany) with an Ultra Turrax (IKA Labortechnik, Staufen, Germany). The total RNA of callus and midshaft samples and periosteal cell suspensions was isolated using columns of a NucleoSpin RNA kit (Macherey-Nagel, Düren, Germany). Concentration and quality of the derived RNA was monitored by using NanoDrop 2000 system (NanoDrop Technology). Reverse transcription into cDNA was performed using a cDNA synthesis kit (ProtoScript First Strand cDNA Synthesis Kit, New England BioLabs, Ipswich, Massachusetts, USA) according to the manufacturer's instructions. Quantitative real-time PCR was conducted using TaqMan Assay-on-Demand primer sets (Applied Biosystems by Thermo Fisher Scientific, Waltham, Massachusetts, USA) or Power SYBR Green PCR Master Mix (Merck, KGaA, Darmstadt, Germany). Primers used for TaqMan included the following: *Alpl* (Mm00475834_m1), *Atf4* (Mm00515325_g1), *Bglap* (Mm03413826_mH), *Calcr* (Mm00432271_m1), *Cd68* (Mm03047342_m1), *Ctsk* (Mm00484039_m1), *Dmp1* (Mm01208363_m1), *Gapdh* (Mm99999915_g1), *Hif1a* (Mm00468869_m1), *Mmp13* (Mm00439491_m1), *Ucp1* (Mm01244861_m1), *Vegfa* (Mm00437306_m1). Primers for SYBR Green were designed as follows: *Gapdh* (FOR-TGCACCAACTGCTTAG, REV-GGATGCAGGGATGATGTTC), *Pdgfrb* (FOR-AGTGAGGACAGACGTCCCAT, REV-GAGGTGGTAATCCCGTCAGC), *Slc6a2* (FOR-TGTGTTTGTACGCCCAGGTG, REV-ACCTCCTAGCACCTT

CGTGA). For all groups, values are displayed as expression over the housekeeping gene Glyceraldehyde-3-phosphate dehydrogenase (*Gapdh*) as a reference. The ΔΔCT method was used for relative quantification.

ELISA

Serum NE levels were measured by ELISA (BA-E-5200R, Immusmol, Bordeaux, France) according to the manufacturer's protocol.

QUANTIFICATION AND STATISTICAL ANALYSIS

The sample size was calculated for the main outcome parameter callus mineral content derived by μCT analysis, yielding a minimum required number of n = 5 mice per group. To account for occasional loss of samples after surgery (e.g., dislocation of fracture fixation) or histologic processing (overall not encountered in this study), group size was increased to n = 6 per group and time point for all *in vivo* assays. For *in vitro* studies, n = 6 independent cell cultures were employed. All groups were assigned randomly, and researchers were blinded during sample processing and analyses of outcome measurements. Unpaired two-tailed Students t-Test was used to determine differences between reboxetine and vehicle groups in μCT, histomorphometry, and biomechanical analysis. Non-parametric Mann–Whitney U test was used to analyze gene expression. Results are displayed as box plots with median value and minimum and maximum whiskers. All statistical details of the experiments can be found in the figure legends. At $p < 0.05$, differences were considered statistically significant (GraphPad Prism 6, La Jolla, CA, USA).